Translocation of ^{133}Cs administered to *Cryptomeria japonica* wood

Dan Aoki[a,*], Ryutaro Asai[a], Rie Tomioka[a], Yasuyuki Matsushita[a], Hiroyuki Asakura[b,c], Masao Tabuchi[d], Kazuhiko Fukushima[a]

[a] Graduate School of Bioagricultural Sciences, Nagoya University, Furo-cho, Chikusa-ku, Nagoya, Aichi 464-8601, Japan

[b] Elements Strategy Initiative for Catalysts & Batteries (ESICB), Kyoto University, 1-30 Goryo-Ohara, Nishikyo-ku, Kyoto 615-8245, Japan

[c] Department of Molecular Engineering, Graduate School of Engineering, Kyoto University, Kyotodaigaku Katsura, Nishikyo-ku, Kyoto 615-8510, Japan

[d] Synchrotron Radiation Research Center, Nagoya University, Furo-Cho, Chikusa-Ku, Nagoya 464-8603, Japan

* Corresponding author

Tel: +81-52-789-4062

Fax: +81-52-789-4163

E-mail address: daoki@agr.nagoya-u.ac.jp

Abstract

To reveal the *in planta* behaviour of caesium (Cs), the stable isotope ^{133}Cs was administered into 3-year-old *Cryptomeria japonica* seedlings by the application of ^{133}CsCl aqueous solution to the bark surface. The administered ^{133}Cs was quantified by ICP-MS measurements, which showed transportation of ^{133}Cs in an ascending direction in the stem. Distribution of ^{133}Cs was visualized using freeze-fixed *C. japonica* woody stem samples and cryo-time-of-flight secondary ion mass spectrometry/scanning electron microscopy (cryo-TOF-SIMS/SEM) analysis. Cryo-TOF-SIMS/SEM visualization suggested that ^{133}Cs was rapidly transported radially by ray parenchyma cells followed by axial transportation by pith and axial parenchyma cells. Adsorption experiments using powdered *C. japonica* wood samples and X-ray absorption fine structure (XAFS) analysis suggested that ^{133}Cs was in the hydrated state following its deposition into tracheid cell walls.

Keywords: ^{133}Cs; Cryptomeria japonica; cryo-TOF-SIMS; ICP-MS; XAFS

1. Introduction

The Fukushima Daiichi Nuclear Power Plant (FDNPP) accident in March 2011 released various radionuclides and contaminated an expansive area of eastern Japan, with concentrated fallout primarily in the Fukushima prefecture [Japanese Ministry of Education, Culture, Sports, Science, and Technology, 2011; Hashimoto et al., 2012; Kinoshita et al., 2011; Yoshida et al., 2012]. Importantly, ^{137}Cs, the radioactive isotope of caesium, has a long half-life period and its impact on crop production [Endo et al., 2013; Hiraide et al., 2015; Kiyono et al., 2013, Mori et al., 2012, Nobori et al., 2016, Ohmori et al., 2014a, 2014b, Okuda et al., 2013], the livestock industry [Fukuda et al., 2013; Iguchi et al., 2013], and forest ecosystems [Avila et al., 2001; Baeza et al., 2005; Fujii et al., 2014; Hashimoto et al., 2013; Mahara et al., 2014; Yasunari et al., 2011; Yoschenko et al., 2016; Yoshida et al., 2004] is a serious concern. The environmental behaviour of ^{137}Cs should be adequately described for current and future management practices.

Japanese cedar, *Cryptomeria japonica* D. Don, is the most abundant conifer in the forest plantations of the Fukushima prefecture [Ministry of Agriculture, Forestry and Fisheries of Japan, 2012]. The levels of radioactivity in *C. japonica* wood have been analysed following the accident. Several research groups measured the ^{137}Cs concentration in samples of *C. japonica* bark, sapwood, and heartwood and suggested that FDNPP-derived ^{137}Cs was partially absorbed through the foliage and rapidly translocated into the wood of these trees [Kuroda et al., 2013a; Ohashi et al., 2014]. Concerning the *in planta* transportation of ^{137}Cs, several studies have reported that the newly formed needles and pollen of *C. japonica* contained ^{137}Cs [Akama et al., 2013; Kanasashi et al., 2015; Nishikiori et al., 2015]. $^{133/134/137}$Cs (Cs) uptake via the bark [Sasaki et al., 2016; Wang et al., 2016] and roots [Chu et al., 2015; Ertel and Ziegler 1991; Fesenko et al., 2001; Gommers et al., 2005] were also documented. It is apparent from these reports that Cs are absorbed into and translocated within wood. The transportation mechanism of Cs has been considered as generally similar to that of potassium (K) [Sombré et al., 1994; Sugiura et al., 2016; Yoshihara et al., 2014; White and Broadley 2000; Zhu and Smolders 2000]. However, it has been suggested that the *in planta* distribution and transport dynamics of ^{137}Cs and K are not completely alike [Buysse, et al., 1995; Goor and Thiry, 2004; Kobayashi et al., 2016; Rantavaara et al., 2012]. It was also alerted to that the insufficient appreciation of the detailed *in planta* translocation of Cs should cause the over and/or under estimation of the environmental transfer factors of Cs [Goor and Thiry, 2004].

Based on previous studies, it is thought that Cs may be transported in the water-soluble cation state in the plant. Although the radial and axial mobility of Cs in several wood species is well recognized [Momoshima et al., 1994, Okada et al., 1993, Thiry et al., 2002], there are few documented reports of the anatomical wood properties which sustain the Cs transport. The objective of this study is to characterize the transportation and final location of Cs absorbed into living trees.

It is important to understand the mechanisms behind *in planta* Cs translocation and the final chemical state of the absorbed water-soluble Cs in order to develop forest and wood product decontamination strategies and for future management of the forest.

One of the major difficulties in analysing Cs transportation in woody stems is the water-soluble nature of Cs. The pre-treatment process for microscopic observation, which includes cutting, sectioning, embedding, and drying, can alter the specific *in planta* distribution of water-soluble chemicals. Therefore, plant samples should be frozen and analysed without defrosting. Cryo-scanning electron microscopy with energy dispersive X-ray spectroscopy (cryo-SEM-EDX) is a potential technique to visualize such a water-soluble heavy metal absorbed into living plant tissue. However, the detection limit of Cs in EDX analysis is reported as ~0.01 % [Groenewold and Ingram 1998] and it is potentially difficult to visualize the early stages of Cs transportation in the plant. To characterise *in planta* Cs transportation, cryo time-of-flight secondary ion mass spectrometry (cryo-TOF-SIMS)/SEM was used in this study. TOF-SIMS has significantly higher sensitivity for alkaline metals than that of SEM-EDX [Heard et al., 2001]. The lower spatial resolution of cryo-TOF-SIMS can be compensated by parallel analysis of the same sample using cryo-SEM [Aoki et al., 2016, Metzner et al., 2008]. The detection limit of TOF-SIMS remains insufficient to visualize trace amounts of ^{137}Cs. Nevertheless, it has been reported that the behaviours of ^{133}Cs and ^{137}Cs are similar when both species are in a water-soluble state [Okuda et al., 2012, 2013; Yoshida et al., 2004].

In this study, the stable ^{133}Cs isotope was administered into *C. japonica* wood samples via their bark and roots. The absorbed ^{133}Cs was quantified by inductively coupled plasma mass spectrometry (ICP-MS) and, based on the above reasoning, the *in planta* ^{133}Cs transportation was visualized by cryo-TOF-SIMS/SEM analysis. The chemical form of ^{133}Cs adsorbed onto powdered wood was examined by X-ray absorption fine structure (XAFS) analysis using synchrotron radiation.

2. Materials and methods

2.1. Preparation of *C. japonica* samples administered with ^{133}Cs

Experimental samples were potted seedlings of 3-year-old *C. japonica*, which had a total height of 1.2 m and an 8–12 mm diameter at 40 cm from the base of the stem. The peat moss soil for raising seedlings (TH-1, Oji Forest & Products Co., Ltd., Japan) was used and the pot volume was 3.6 L for each. For administration of ^{133}Cs into the bark, absorbent cotton was bound to the stem at 40 cm from its base and the application area selected did not contain any nodes or damaged tissue. 100 mM ^{133}CsClaq was applied onto the cotton at noon each day, ensuring that no solution spread to other bark areas. For administration of ^{133}Cs into the roots, 35 mL of 100-mM ^{133}CsClaq

was applied onto the soil at noon each day.

The seedlings were grown in a temperature-controlled room with a light environment created using LEDs (VEFA140WZN, 130W, Altrader). The photoperiod was 12 h and room temperature ranged from 20–25°C. Samples from those seedlings administered ^{133}Cs into the bark were collected 8 h, 24 h, 48 h, and 12 days following the commencement of treatment. An additional sample, denoted 48h+1month, was created by applying ^{133}CsClaq as described above to the bark of a seedling for 48 h followed by a further one month of growth without any additional ^{133}Cs administration. The seedling administered ^{133}Cs into the roots was sampled following 9 days of treatment and denoted root-9d.

Wood samples were cut from the stems of seedlings to obtain 10-mm-thick sample disks from positions at 20 cm, 40 cm, 60 cm, 80 cm, and 100 cm from the base of the stem. The sample disk was cut into small blocks (circular sector of radius 6–8 mm and central angle of $\pi/8$) containing the bark, cambial zone, xylem, and pith. The divided sample blocks were quick-frozen with liquid Freon R22 (DuPont) at −160°C and stored at −80°C before further use. Samples were labelled according to their ^{133}Cs administration period and sampling height (e.g. 8h-40cm). Needles at 60 cm from the base and at the top of seedlings and cones at the top of seedlings were also sampled. Seedling cultivation was conducted from September to October 2014.

2.2. ^{133}Cs quantification using ICP-MS

The frozen sample block were cut by sliding microtome at −20°C to obtain 100 μm radial sections containing bark, xylem, and pith tissue. Freeze-dried radial sections (0.1 g in total for each measurement) were treated using the wet ashing method under the following conditions: 160°C for 1 h and 220°C for 2 h with 15 mL HNO_3. The resulting sample solution was diluted to 50 mL and analysed using an ICP-MS instrument (Agilent 7500, Agilent Technologies). Indium and rhodium were added and used as internal standards.

2.3. Cryo-TOF-SIMS/SEM analysis

The frozen sample block was fixed on the sample holder and cut by sliding microtome at −30°C in a glove box filled with dry and cooled nitrogen gas. The resulting fresh and flat transverse surface of the sample was used for subsequent analysis. The sample holder was transferred to the cryo-TOF-SIMS by a cryo-vacuum transfer shuttle. The details of the cryo-TOF-SIMS/SEM system have been reported previously [Kuroda et al., 2013b; Masumi et al., 2014].

Cryo-TOF-SIMS measurements were conducted using a TRIFT III spectrometer (ULVAC-PHI, Inc.). Positive ion spectra were obtained under the following conditions: primary ion of 22 keV Au_1^+ at a current of 5 nA, raster size of 400 μm × 400 μm, pulse width of 1.8 ns (bunched for

spectrum mode) or 13.0 ns (not bunched for image mode), mass range of *m*/*z* 0–1850, spot size of 1.0 μm in image mode, temperature of −120 to −130°C, and a low-energy pulsed electron ion gun (30.0 eV) which was used for surface charge compensation. All images accumulated approximately 2,000,000 secondary ion counts and primary ion doses for the each sample surface were 1.0–1.5E+9/cm^2. Obtained images were connected using WinCadence 5.1.2.8 (ULVAC-PHI Inc.) and MatLab R2014a (The MathWorks, Inc.) with PLS Toolbox 7.5.2 (Eigenvector Research, Inc.), and the colour scale was changed using ImageJ software (The National Institutes of Health, USA).

Following cryo-TOF-SIMS measurements, the same region was observed by cryo-SEM (S-3400N, Hitachi High-Technologies Corporation). To enhance the image contrast, appropriate freeze-etching was carried out at −90°C before the observation. The observation conditions were as follows: acceleration voltage of 1.5 kV, temperature of −120°C, and a working distance of 10 mm. Overlaid images of the selected cryo-TOF-SIMS ion on cryo-SEM image were prepared using Photoshop CS5 Extended (Adobe Systems Incorporated).

2.4. XAFS measurements

XAFS experiments were conducted at beam line BL5S1 of the Aichi Synchrotron Radiation Centre (Tabuchi et al. 2016) for ^{133}Cs-L3 adsorption edge by transmission mode. Ion chambers filled with gases of He:N2 = 70:30 and Ar:N2 = 15:85 were used as detectors to measure incident and transmitted X-ray intensity. Typically, approximately 40 min was required to measure one spectrum. The photon energy was calibrated using the pre-edge peak (4966 eV) of Ti K-edge. Standard ^{133}Cs samples (^{133}CsCl and ^{133}CsOH) were mixed with boron nitride under an atmosphere of argon, pressed to form a tablet, and measured in an encapsulated state in a polyethylene pouch to avoid the absorption of moisture. Wood samples were freeze-dried before they were measured.

To prepare the standard wood samples containing ^{133}Cs, sapwood of *C. japonica* was ball-milled and the resulting powdered wood was used. Powdered wood (0.3 g dry weight) was suspended in 30 mL of 100 mM ^{133}CsCl or ^{133}CsOH aqueous solutions. The mixture was agitated at room temperature for 30 minutes. The powdered wood was filtered out of solution, subjected to five washes in water, and freeze-dried. Standard powdered wood samples were pressed to form a tablet before they were measured. Obtained data were processed using Athena software (ver. 0.9.18) included in the Demeter package [Ravel and Newville 2005].

3. Results and Discussion

3.1. Quantification of adsorbed ^{133}Cs

Following the designated time periods, samples taken from the *C. japonica* seedlings were submitted to ICP-MS quantification. The obtained results are summarized in Fig. 1. ^{133}Cs detection

was minimal in the control sample that was not administered ^{133}CsClaq. In those seedlings administered ^{133}CsClaq, ^{133}Cs was detected in wood samples and the amount was largely proportional to the length of the administration period. In those samples taken at 40 cm from the base of the seedling, significant levels of ^{133}Cs were detected for all administration periods, suggesting that most of the administered ^{133}Cs remained in the bark. In those samples taken at 60–100 cm from the base of the seedling, the amount of ^{133}Cs detected gradually decreased with increased sampling height. In comparison with those samples above the ^{133}Cs application area, those samples taken at 20 cm from the base of the seedling displayed less ^{133}Cs content with the exception of the root-9d sample. The amount of ^{133}Cs detected in the root-9d samples gradually decreased with increased sampling height. Regarding needle and cone samples, ^{133}Cs amount in needles at 60 cm from the base of the seedling was lower than that of the stem samples at 60–100 cm sampling height. Following the longest administration period of 12 days, needle and cone samples at the top of the seedling showed high ^{133}Cs content, while needles at 60 cm sampling height contained minimal ^{133}Cs.

Thus, ^{133}Cs transportation in the experimental seedlings may be briefly summarised as follows: the administered ^{133}Cs was transferred to an ascending direction of the seedling. ^{133}Cs tends to be transferred to needles and cones at the top rather than to needles at middle heights of the seedling. After the administration of large volumes of ^{133}Cs (12d), internal ^{133}Cs concentrations in the plant was high. From these results, it was confirmed that the administered ^{133}Cs was successfully absorbed into *C. japonica* wood.

3.2. Cryo-TOF-SIMS visualization of ^{133}Cs in freeze-fixed *C. japonica* wood

TOF-SIMS has two measurement modes, namely image mode, which has higher lateral resolution and lower mass resolution, and contrary spectrum mode. A typical cryo-TOF-SIMS spectrum obtained for a ^{133}Cs-administered sample is displayed in Fig. 2. In the spectrum, mass to charge ratio (*m*/*z*) 19 ion is $[H_3O]^+$, which suggests the sample surface is in a frozen-hydrated state. K^+ of *m*/*z* 39 and $^{133}Cs^+$ of *m*/*z* 133 were also detected. For K^+ and $^{133}Cs^+$ ion mapping, we examined the mass resolution of both measurement modes. As shown in Fig. 2, K^+ and $^{133}Cs^+$ were clearly separated in spectrum mode measurements (Fig. 2b, 3c), and it was also possible to distinguish their signals in image mode measurements (Fig. 2d, 3e). To discuss ^{133}Cs distribution in more detail with reference to the cell and tissue classification, K^+ and $^{133}Cs^+$ mapping are hereafter displayed with image mode measurements (Fig. 2d, 3e, grey regions were used).

Fig. 3 shows (a) total ion, (b) K^+, and (c) $^{133}Cs^+$ images of the 8h-40 cm sample (height of ^{133}CsClaq administration). Furthermore, the ion images of K^+ and $^{133}Cs^+$ were overlaid onto the cryo-SEM images to clarify their distribution (Fig. 3d, 3e, 3f, and 3g). K^+ was detected only in the

living inner bark tissue. On the other hand, $^{133}Cs^{+}$ was strongly detected in the outer bark region as a result of the administration. The $^{133}Cs^{+}$ permeation rate seems to be reduced at the boundary between outer bark and inner bark tissue. The result might suggest that the permeation mechanism changed from simple diffusion to biological permeation at the boundary (Fig. 3e). In the inner bark, cambial zone, and differentiating xylem tissue, $^{133}Cs^{+}$ was seldom detected. However, $^{133}Cs^{+}$ was clearly detected at the innermost part of the pith (Fig. 3c and 3g).

Based on these results, we concluded that ^{133}Cs was transported from bark to pith within 8 h of administration. Although there were no significant amounts of $^{133}Cs^{+}$ detected in the intermediate region, the possible route of transportation may be ray parenchyma cells, which is discussed further below. Rapid transportation of the alkali metal rubidium via ray parenchyma cells has also been reported [Okada et al., 2011, 2012]. The absence of ^{133}Cs in the intermediate region may be interpreted by considering rate of transport; the radial transportation of ^{133}Cs via ray parenchyma cells is potentially faster than the permeation of ^{133}Cs from outer bark to inner bark. Consequently, the concentration of ^{133}Cs in ray parenchyma cells of the intermediate region might not be sufficient for cryo-TOF-SIMS visualization.

The next stage of ^{133}Cs transportation was analysed by the cryo-TOF-SIMS measurement of $^{133}Cs^{+}$ in 8h-60 cm, 48h-60 cm, and 48h-20 cm samples (Fig. 4). Concerning samples taken from above the site of administration (8h-60 cm), the transportation of ^{133}Cs from the pith in an outward direction was clearly visualized (Fig. 4b). This result suggests that within 8 h following administration, ^{133}Cs is able to be transported from the bark to the pith and then transported further to elevated tissue via the pith. Following 48-h of ^{133}Cs administration, $^{133}Cs^{+}$ was distributed throughout the tissue section in those samples taken at 60 cm seedling height (Fig. 4d). Conversely, $^{133}Cs^{+}$ detection was less at a lower seedling height position (Fig. 4f). However, $^{133}Cs^{+}$ axial transportation in the pith was indicated slightly in lower seedling height samples following 48 h of ^{133}Cs administration (Fig. 4f). These cryo-TOF-SIMS images suggest that administered ^{133}Cs could be transported in an axial direction in the pith region. The ascending nature of ^{133}Cs transportation agreed with the ICP-MS result (Fig. 1).

Following a long administration period, ^{133}Cs was absorbed more into the sample and the adsorbed $^{133}Cs^{+}$ was clearly visualized as shown in Fig. 5. ^{133}Cs was deposited on ray parenchyma cells as displayed in Fig. 5d, which supports the hypothesis of ^{133}Cs transportation via ray parenchyma cells. Additionally, highly concentrated ^{133}Cs was observed in axial parenchyma cells (Fig. 5f). It can thus be proposed that axial parenchyma cells contribute to the axial transportation of ^{133}Cs in xylem.

In this study, the early radial movement of ^{133}Cs was associated with ray parenchyma cells and pith. It was also suggested that axial parenchyma cells contribute the axial transportation of ^{133}Cs.

The ascending trend should be driven by these phenomena. After the certain period, ^{133}Cs was detected strongly in the inner bark region in either case of the ^{133}Cs administration via their bark or roots (Fig. 5a and 5b). Previous study suggested that the *in planta* transportation of ^{137}Cs should be driven by the downward movement via the inner bark region and the upward transport in the xylem region [Buysse, et al., 1995; Goor and Thiry, 2004; Kobayashi et al., 2016; Rantavaara et al., 2012; Thiry et al., 2002]. Such mixing and recycling behaviour of ^{137}Cs agreed with the result of the present study using ^{133}Cs.

As for the ^{133}Cs deposition in the xylem region, ^{133}Cs was rapidly transported into the pith and the apparent ^{133}Cs concentration in ray parenchyma cells should be low at the early stage as depicted in Fig. 3. Subsequently, ^{133}Cs seemed to be deposited on ray parenchyma cells or increased in concentration in ray parenchyma cells. Following this, ^{133}Cs diffused into neighbouring tracheid cells and finally was distributed throughout the entire wood tissue.

Based on these results, we hypothesized that the deposition of ^{133}Cs into lignified tracheid cells, the main structure of wood xylem, is most likely via simple permeation of ^{133}Cs in the water-soluble state, because the lignified tracheid cells perform no biological function. Thus, it may be possible to simulate the deposition of ^{133}Cs into the wood cell walls by simple experiments whereby powdered wood samples and water-soluble ^{133}Cs are mixed. The majority of wood biomass is xylem tissue and knowledge of the chemical form of ^{133}Cs deposited onto xylem cells is expected to play an important role in developing decontamination techniques and safe usage methods for ^{137}Cs-contaminated wood. To examine the chemical form of ^{133}Cs in wood xylem tissue, XAFS measurements were conducted using ^{133}Cs and powdered wood samples.

3.3. XAFS analysis of adsorbed ^{133}Cs

There are several reports studying the chemical form of Cs adsorbed to variable matrices using XAFS analysis. Cs can be trapped in clay minerals and form inner-sphere complexes [Bostick et al., 2002; Fan et al., 2014a, 2014b; Kemner et al., 1997; Tanaka et al., 2013]. It was also reported that Cs is able to form complexes with organics such as crown ethers [Kemner et al., 1996]. Thus, XAFS analyses offer useful information concerning the chemical form of Cs.

In this study, XAFS analysis was applied to wood samples containing ^{133}Cs. The ^{133}Cs-administered wood samples were also measured but the concentration of ^{133}Cs was too low to analyse its chemical form in detail. Using the ^{133}Cs-adsorbed powdered wood samples and ^{133}Cs standards, we obtained ^{133}Cs-L_3 edge X-ray absorption near edge structure spectra, k^2-weighted ^{133}Cs-L_3 extended XAFS spectra, and their Fourier transforms as are shown in Fig. 6. In Fig. 6a, the ^{133}Cs-L_3 edge was clearly displayed. ^{133}Cs adsorbed to powdered wood displayed a similar result to that of ^{133}CsOH regardless of whether the powered wood was immersed

into ^{133}CsClaq or ^{133}CsOHaq (Fig. 6b). In Fig. 6c, the major peak at R = 2–3 likely suggests a link with the nearest oxygen–meaning an outer-sphere complex–and corresponds to that of hydrated ^{133}Cs as previously reported for the ^{133}Cs-mineral complex samples [Fan et al., 2014a; Tanaka et al., 2013; Qin et al., 2012]. If ^{133}Cs formed an inner-sphere complex as reported for clay minerals [Bostick et al., 2002; Fan et al., 2014a, 2014b; Kemner et al., 1997; Tanaka et al., 2013] and crown ethers [Kemner et al., 1996], the second peak should occur at R = 3–4. However, ^{133}Cs adsorbed to powdered wood did not exhibit such a peak. These results suggest that the adsorbed ^{133}Cs in dried wood xylem was not ^{133}CsCl and might be in a hydrated state. The possible adsorbent may be alcoholic or phenolic OH groups in the plant cell wall matrix.

4. Conclusions

Stable ^{133}Cs isotope was administered into *C. japonica* wood samples via the bark and roots. The administered ^{133}Cs was absorbed into woody stems and was transported in an ascending direction in the stem. Cryo-TOF-SIMS/SEM visualization of administered ^{133}Cs suggested that rapid radial transportation of ^{133}Cs occurred via ray parenchyma cells, followed by axial transportation via pith and axial parenchyma cells. In this study, 3-year-old seedlings were used and, thus, the results should be applicable to saplings and branches of mature wood in an existing forest. XAFS analysis suggested that ^{133}Cs was in a hydrated state following deposition into xylem cell walls. Chemical treatments that result in delignification, fibrillation, and alkali metal recovery, such as a kraft pulping, might be an effective approach to safely use the ^{137}Cs-contaminated wood xylem.

Acknowledgements

The authors thank Morimoto H for help with XAFS measurements, Wang W for help with ^{133}Cs administration experiments, Kuroda K for cryo-TOF-SIMS/SEM experimental suggestions. This work was supported by Grant-in-Aid for Scientific Research (25252032, 25110507, and 15K00975) from the Ministry of Education, Culture, Sports, Science and Technology (MEXT) of Japan. The XAFS experiments were conducted at the BL5S1 of Aichi Synchrotron Radiation Centre, Aichi Science & Technology Foundation, Aichi, Japan (Proposal No. 2503065 and 2014LA007) and financially supported by the Nagoya University Synchrotron Radiation Research Center.

References

Akama A, Kiyono Y, Kanazashi T, Shichi K. Survey of radioactive contamination of sugi (*Cryptomeria japonica* D. Don) shoots and male flowers in Fukushima prefecture. Jpn J For Environ 2013: 55: 105–111.

Aoki D, Hanaya Y, Akita T, Matsushita Y, Yoshida M, Kuroda K, Yagami S, Takam R, Fukushima K. Distribution of coniferin in freeze-fixed stem of *Ginkgo biloba* L. by cryo-TOF-SIMS/SEM. Sci Rep 2016: 6: 31525.

Avila R, Bergman R, Scimone M, Fesenko S, Sancharova N, Moberg L. A comparison of three models of ^{137}Cs transfer in forest ecosystems. J Environ Radioact 2001: 55: 315–327.

Baeza A, Guillén J, Bernedo JM. Soilefungi transfer coefficients: Importance of the location of mycelium in soil and of the differential availability of radionuclides in soil fractions. J Environ Radioact 2005: 81: 89–106.

Bostick BC, Vairavamurthy MA, Karthikeyan KG, Chorover J. Cesium Adsorption on Clay Minerals: An EXAFS Spectroscopic Investigation. Environ Sci Technol 2002: 36: 2670–2676.

Buysse J, van der Brande K, Merckx R. The distribution of radiocesium and potassium in Spinach plants grown at different shoot temperatures. J Plant Physiol 1995: 146: 263–267.

Chu Q, Watanabe T, Sha Z, Osaki M, Shinano T. Interactions between Cs, Sr, and Other Nutrients and Trace Element Accumulation in Amaranthus Shoot in Response to Variety Effect. J Agr Food Chem 2015: 63: 2355–2363.

Endo S, Kajimoto T, Shizuma K. Paddy-field contamination with ^{134}Cs and ^{137}Cs due to Fukushima Dai-ichi Nuclear Power Plant accident and soil-to-rice transfer coefficients. J Environ Radioact 2013: 116: 59–64

Ertel J. Ziegler H. Cs-134/137 contamination and root uptake of different forest trees before and after the Chernobyl accident. Radiat Environ Biophys 1991: 30: 147–157.

Fan Q, Yamaguchi N, Tanaka M, Tsukada H, Takahashi Y. Relationship between the adsorption species of cesium and radiocesium interception potential in soils and minerals: an EXAFS study. J Environ Radioact 2014b: 138: 92–100.

Fan QH, Tanaka M, Tanaka K, Sakaguchi A, Takahashi Y. An EXAFS study on the effects of natural organic matter and the expandability of clay minerals on cesium adsorption and mobility. Geochim Cosmochim Acta 2014a: 135: 49–65.

Fesenko SV, Soukhova NV. Sanzharova NI, Avila R, Spiridonov SI, Klein D, Lucot E, Badot P-M. Identification of processes governing long-term accumulation of ^{137}Cs by forest trees following the Chernobyl accident. Radiat Environ Biophys 2001: 40: 105–113.

Fujii K, Ikeda S, Akama A, Komatsu M, Takahashi M, Kaneko S. Vertical migration of radiocesium and clay mineral composition in five forest soils contaminated by the Fukushima nuclear accident. Soil Sci Plant Nut 2014: 60: 751–764.

Fukuda T, Kino Y, Abe Y, Yamashiro H, Kuwahara Y, Nihei H, Sano Y, Irisawa A, Shimura T, Fukumoto M, Shinoda H, Obata Y, Saigusa S, Sekine T, Isogai E, Fukumoto M. Distribution of Artificial Radionuclides in Abandoned Cattle in the Evacuation Zone of the Fukushima Daiichi Nuclear Power Plant. PLOS ONE 2013: 8: e54312.

Gommers A, Gäfvert T, Smolders E, Merckx R, Vandenhove H. Radiocaesium soil-to-wood transfer in commercial willow short rotation coppice on contaminated farm land. J Environ Radioact 2005: 78: 267–287.

Goor F, Thiry Y, Processes, dynamics and modelling of radiocaesium cycling in a chronosequence of Chernobyl-contaminated Scots pine (Pinus sylvestris L.) plantations. Sci Total Environ 2004: 325: 163–180.

Groenewold GS, Ingram JC, Cs^+ Speciation on Soil Particles by TOF-SIMS Imaging. Anal Chem 1998: 70: 534–539.

Hashimoto S, Matsuura T, Nanko K, Linkov I, Shaw G, Kaneko S. Predicted spatio-temporal dynamics of radiocesium deposited onto forests following the Fukushima nuclear accident. Sci Rep 2013: 3: 2564.

Hashimoto S, Ugawa S, Nanko K, Shichi K. The total amounts of radioactively contaminated materials in forests in Fukushima, Japan. Sci Rep 2012: 2: 416.

Heard PJ, Feeney KA, Allen GC, Shewry PR. Determination of the elemental composition of mature wheat grain using a modified secondary ion mass spectrometer (SIMS). Plant J 2001: 30: 237–245.

Hiraide M, Sunagawa M, Neda H, Humaira N, Abdullah L. Yoshida S. Reducing radioactive cesium transfer from sawdust media to *Pleurotus ostreatus* fruiting bodies. J Wood Sci 2015: 61: 420–430.

Iguchi K, Fujimoto K, Kaeriyama H, Tomiya A, Enomoto M, Abe S, Ishida T. Cesium-137 discharge into the freshwater fishery ground of grazing fish, ayu *Plecoglossus altivelis* after the March 2011 Fukushima nuclear accident. Fish Sci 2013: 79: 983–988.

Japanese Ministry of Education, Culture, Sports, Science, and Technology. Results of the Fourth Airborne Monitoring Survey by MEXT, http://radioactivity.nsr.go.jp/en/contents/4000/3179/24/1270_1216.pdf (accessed 10.10.16).

Kanasashi T, Sugiura Y, Takenaka C, Hijii N, Umemura M. Radiocesium distribution in sugi (*Cryptomeria japonica*) in Eastern Japan: translocation from needles to pollen. J Environ Radioact 2015: 139: 398–406.

Kemner K, Hunter D, Bertsch P, Kirkland J, Elam W. Determination of Site Specific Binding Environments of Surface Sorbed Cesium on Clay Minerals by Cs-EXAFS. J Phys IV 1997: 7: C2-777–C2-779.

Kemner KM, Hunter DB, Elam WT, Bertsch PM. XAFS Studies of Solution-Phase Complexes of Cesium with Dibenzo-18-crown-6 Ethers. J Phys Chem 1996: 100: 11698–11703.

Kinoshita N, Sueki K, Sasa K, Kitagawa J, Ikarashi S, Nishimura T, Wong YS, Satou Y, Handa K, Takahashi T, Sato M, Yamagata T. Assessment of individual radionuclide distributions from the Fukushima nuclear accident covering central-east Japan. PNAS 2011: 108: 19526–19529.

Kiyono Y, Akama A. Radioactive cesium contamination of edible wild plants after the accident at the Fukushima Daiichi Nuclear Power Plant. Jpn J For Environ 2013: 55: 113–118

Kobayashi NI, Sugita R, Nobori T, Tanoi K, Nakanishi TM. Tracer experiment using $^{42}K^{+}$ and $^{137}Cs^{+}$ revealed the different transport rates of potassium and caesium within rice roots. Funct Plant Biol 2016: 43: 151–160.

Kuroda K, Fujiwara R, Imai T, Takama R, Saito K, Matsushita Y, Fukushima K. The cryo-TOF-SIMS/SEM system for the analysis of the chemical distribution in freeze-fixed *Cryptomeria japonica* wood. Surf Interface Anal 2013b: 45: 215–219.

Kuroda K, Kagawa A, Tonosaki M. Radiocesium concentrations in the bark, sapwood and heartwood of three tree species collected at Fukushima forests half a year after the Fukushima Dai-ichi nuclear accident. J Environ Radioact 2013a: 122: 37–42.

Mahara Y, Ohta T, Ogawa H. Kumata A. Atmospheric Direct Uptake and Long-term Fate of Radiocesium in Trees after the Fukushima Nuclear Accident. Sci Rep 2014: 4: 7121.

Masumi T, Matsushita Y, Aoki D, Takama R, Saito K, Kuroda K, Fukushima K. Adsorption behavior of poly(dimethyl-diallylammonium chloride) on pulp fiber studied by cryo-time-of-flight secondary ion mass spectrometry and cryo-scanning electron microscopy. Appl Surf Sci 2014: 289: 155–159.

Metzner R, Schneider HU, Breuer U, Schroeder WH. Imaging Nutrient Distributions in Plant Tissue Using Time-of-Flight Secondary Ion Mass Spectrometry and Scanning Electron Microscopy. Plant Physiol 2008: 147: 1774–1787

Ministry of Agriculture, Forestry and Fisheries of Japan. The 87th Statistical Yearbook of Ministry of Agriculture, Forestry and Fisheries (2011–2012) (in Japanese) 2012. http://www.maff.go.jp/e/tokei/kikaku/nenji_e/87nenji/index.html#nse010 (accessed 10.10.16)

Momoshima N, Eto I, Koguji H, Takashima Y, Koike M, Imaizumi Y, Harada T. Distribution and chemical characteristics of cations in annual rings of Japanese cedar. J Environ Qual 1994: 24: 1141–1149.

Mori S, Hirato A, Tanoi K, Takeda K, Yamakawa T, Nakanishi H. Radioactive cesium flow in *Rhus vernicifera*. Soil Sci Plant Nut 2012: 58: 611–617

Nishikiori T, Watanabe M, Koshikawa K. M, Takamatsu T, Ishii Y, Ito S, Takenaka A, Watanabe K, Hayashi S. Uptake and translocation of radiocesium in cedar leaves following the Fukushima nuclear accident. Sci Total Environ 2015: 502: 611–616.

Nobori T, Kobayashi IN, Tanoi K, Nakanishi M.T. Alteration in caesium behavior in rice caused by the potassium, phosphorous, and nitrogen deficiency. J Radioanal Nucl Chem 2016: 307: 1941–1973.

Ohashi S, Okada N, Tanaka A, Nakai W, Takano S. Radial and vertical distributions of radiocesium in tree stems of *Pinus densiflora* and *Quercus serrata* 1.5 y after the Fukushima nuclear disaster. J Environ Radioact 2014: 134: 54–60.

Ohmori Y, Inui Y, Kajikawa M, Nakata A, Sotta N, Kasai K, Uraguchi S, Tanaka N, Nishida S, Hasegawa T, Sakamoto T, Kawara Y, Aizawa K, Fujita H, Li K, Sawaki N, Oda K, Futagoishi R, Tsusaka T, Takahashi S, Takano J, Wakuta S, Yoshinari A, Uehara M, Takada S, Nagano H, Miwa K, Aibara I, Ojima T, Ebana K, Ishikawa S, Sueyoshi K, Hasegawa H, Mimura T, Mimura M, Kobayashi I.N, Furukawa J, Kobayashi D, Okouchi T, Tanoi K, Fujiwara R. Difference in cesium accumulation among rice cultivars grown in the paddy field in Fukushima Prefecture in 2011 and 2012. J Plant Res 2014: 127: 57–66.

Ohmori Y, Kajikawa N, Nishida S, Tanaka N, Kobayashi N, Tanoi K, Furukawa J, Fujiwara T. The effect of fertilization on cesium concentration of rice grown in a paddy field in Fukushima Prefecture in 2011 and 2012. J Plant Res 2014: 127: 67–71.

Okada N, Hirakawa Y, Katayama Y. Application of activable tracers to investigate radial movement of minerals in the stem of Japanese cedar (*Cryptomeria japonica*). J Wood Sci 2011: 57: 421–428.

Okada N, Hirakawa Y, Katayama Y. Radial movement of sapwood-injected rubidium into heartwood of Japanese cedar (*Cryptomeria japonica*) in the growing period. J Wood Sci 2012: 58: 1–8.

Okada N, Katayama Y, Nobuchi T, Ishimaru Y, Aoki A. Trace elements in the stems of trees VI. Comparisons of radial distributions among hardwood stems. Mokuzai Gakkaishi 1993: 39: 1119–1127.

Okuda M, Hashiguchi T, Joyo M. Tsukamoto K, Endo M, Matsumaru K, Goto-Yamamoto N, Yamaoka H, Suzuki K, Shimoi H. The transfer of radioactive cesium and potassium from rice to sake. J Biosci Bioeng 2013: 116: 340–346.

Okuda M, Joyo M, Tokuoka M, Hashiguchi T, Goto-Yamamoto N, Yamaoka H, Shimoi H. The transfer of stable ^{133}Cs from rice to Japanese sake. J Biosci Bioeng 2012: 114: 600–605.

Qin H, Yokoyama Y, Fan Q, Iwatani H, Tanaka K, Sakaguchi A, Kanai Y, Zhu J, Onda Y, Takahashi Y. Investigation of cesium adsorption on soil and sediment samples from Fukushima Prefecture by sequential extraction and EXAFS technique. Geochem J 2012: 46: 297–302.

Rantavaara A, Vetikko V, Raitio H, Aro L. Seasonal variation of the ^{137}Cs level and its relationship with potassium and carbon levels in conifer needles. Sci Total Environ 2012: 441: 194–208.

Ravel B, Newville M. ATHENA, ARTEMIS, HEPHAESTUS: Data Analysis for X-ray absorption Spectroscopy Using IFEFFIT. J Synchrotron Rad 2005: 12: 537−541.

Sasaki Y. Abe H, Mitachi K, Watanabe Y, Ishii Y, Niizato T. The transfer of radiocesium from the bark to the stemflow of chestnut trees (*Castanea crenata*) contaminated by radionuclides from the Fukushima Dai-ichi nuclear power plant accident. J Environ Radioact 2016: 161: 58–65.

Sombré L, Vanhouche M, de Brouwer S, Ronneau C, Lambotte J.M, Myttenaere C. Long-term radiocesium behaviour in spruce and oak forests. Sci Total Environ 1994: 157: 59–71.

Sugiura Y, Kanasashi T, Ogata Y, Ozawa H, Takenaka C. Radiocesium accumulation properties of *Chengiopanax sciadophylloides*. J Environ Radioact 2016: 151: 250–257.

Tabuchi M, Asakura H, Morimoto H, Watanabe N, Takabe Y. Hard X-ray XAFS beamline, BL5S1, at Aichi SR. J. Phys. Conf. Ser., 2016: 712: 012027.

Tanaka K, Sakaguchi A, Kanai Y, Tsuruta H, Shinohara A, Takahashi Y. Heterogeneous distribution of radiocesium in aerosols, soil and particulate matters emitted by the Fukushima Daiichi Nuclear Power Plant accident: retention of micro-scale heterogeneity during the migration of radiocesium from the air into ground and river systems. J Radioanal Nucl Chem 2013: 295: 1927–1937.

Thiry Y, Goor F, Riesen T. The true distribution and accumulation of radiocaesium in stem of Scots pine (*Pinus sylvestris* L.). J Environ Radioact 2002: 58: 243–259.

Wang W, Hanai Y, Takenaka C, Tomioka R, Iizuka K, Ozawa H. Cesium absorption through bark of Japanese cedar (*Cryptomeria japonica*). J For Res 2016: 21: 251–258.

White PJ, Broadley MR. Mechanisms of caesium uptake by plants. New Phytol 2000: 147: 241–256.

Yasunari TJ, Stohl A, Hayano RS, Burkhart JF, Eckhardt S, Yasunari T. Cesium-137 deposition and contamination of Japanese soils due to the Fukushima nuclear accident. PNAS 2011: 108: 19530–19534.

Yoschenko V, Takase T, Konoplev A, Nanba K, Onda Y, Kiva S, Zheleznyak M, Sato N, Keitoku K. Radiocesium distribution and fluxes in the typical Cryptomeria japonica forest at the late stage after the accident at Fukushima Dai-Ichi Nuclear Power Plant. J Environ Radioact 2016: DOI: 10.1016/j.jenvrad.2016.02.017

Yoshida M, Kanda J, Tracking the Fukushima Radionuclides. Science 2012: 336: 1115–1116.

Yoshida S, Muramatsu Y, Dvornik A.M. Zhuchenko T.A, Linkov I. Equilibrium of radiocesium with stable cesium within the biological cycle of contaminated forest ecosystems. J Environ Radioact 2004: 75: 301–313.

Yoshihara T, Matsumura H, Tsuzaki M, Wakamatsu T, Kobayashi T, Hashida S, Nagaok T, Goto F. Changes in radiocesium contamination from Fukushima in foliar parts of 10 common tree species in Japan between 2011 and 2013. J Environ Radioact 2014: 138: 220–226.

Zhu Y-G, Smolders E. Plant uptake of radiocaesium: a review of mechanisms, regulation and application. J Exp Bot 2000: 51: 1635–1645.

Figure captions

Fig. 1 ^{133}Cs amount in *C. japonica* wood samples as quantified by ICP-MS using freeze-dried radial sections containing bark, xylem, and pith tissue.

Fig. 2 Cryo-TOF-SIMS spectrum of a ^{133}Cs-administered *C. japonica* sample; (a) *m*/*z* 0–200, (b) K^+ and (c) $^{133}Cs^+$ in spectrum mode, (d) K^+ and (e) $^{133}Cs^+$ in image mode. Grey coloured regions were used for the visualization.

Fig. 3 Images obtained by cryo-TOF-SIMS/SEM analysis of the transverse surface of the 8h-40cm sample: cryo-TOF-SIMS ion images of (a) total ion, (b) K^+, (c) $^{133}Cs^+$. (d-e) Cryo-SEM images of bark area (red-square inset in (a)) with $^{133}Cs^+$ (blue) and K^+ (red) overlays (e). (f-g) Cryo-SEM images of pith area (yellow-square inset in (a)) with a $^{133}Cs^+$ (blue) overlay (g).

Fig. 4 Cryo-TOF-SIMS ion images of (a) total ion and (b) $^{133}Cs^+$ ion for 8h-60cm sample, (c) total ion and (d) $^{133}Cs^+$ ion for 48h-60cm sample, and (e) total ion and (f) $^{133}Cs^+$ ion for 48h-20cm sample.

Fig. 5 Cryo-TOF-SIMS images of $^{133}Cs^+$ for (a) 48h1month-60cm sample and (b) root-9d-60cm sample. (c-d) Cryo-SEM images of xylem region (blue-square inset in (a)) with a $^{133}Cs^+$ (blue) overlay (d). (e-f) Cryo-SEM images of xylem region (blue-square inset in (b)) with a $^{133}Cs^+$ (blue) overlay (f). Arrows in (d) and (f) show the positions of ray parenchyma cells (white arrows) and axial parenchyma cells (orange arrows), respectively.

Fig. 6 (a) ^{133}Cs-L_3 edge X-ray absorption near edge structure spectra, (b) k^2-weighted ^{133}Cs-L_3 extended XAFS spectra, and (c) their Fourier transforms obtained for ^{133}CsCl, ^{133}CsOH, and wood samples treated with ^{133}CsClaq or ^{133}CsOHaq.

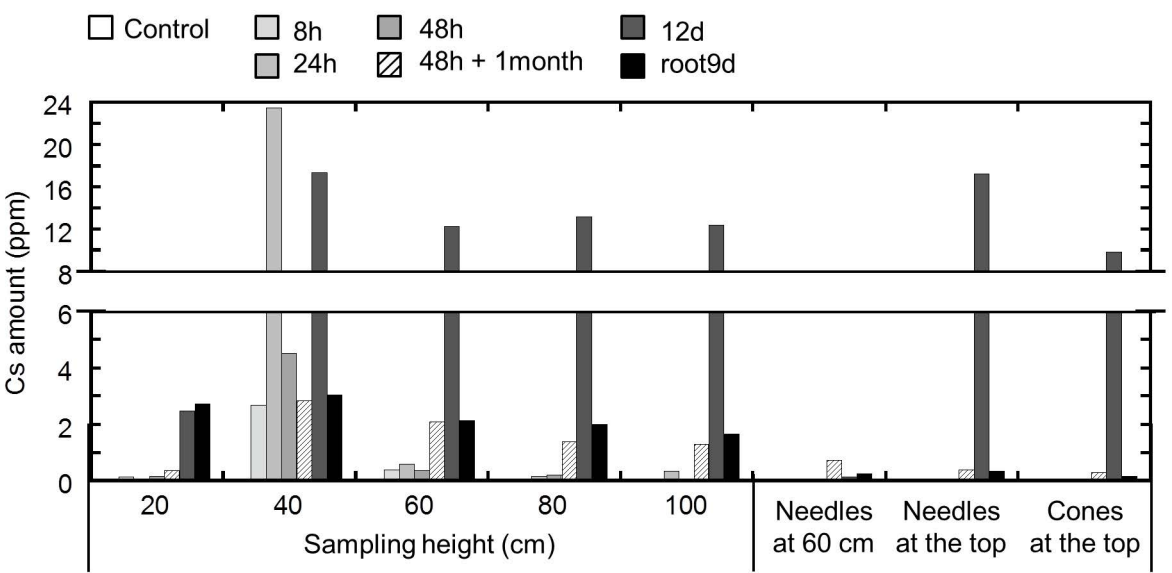
Control
8h
24h
48h
48h + 1month
12d
root9d
Cs amount (ppm)
24
20
16
12
8
6
4
2
0
20
40
60
80
100
Sampling height (cm)
Needles at 60 cm
Needles at the top
Cones at the top

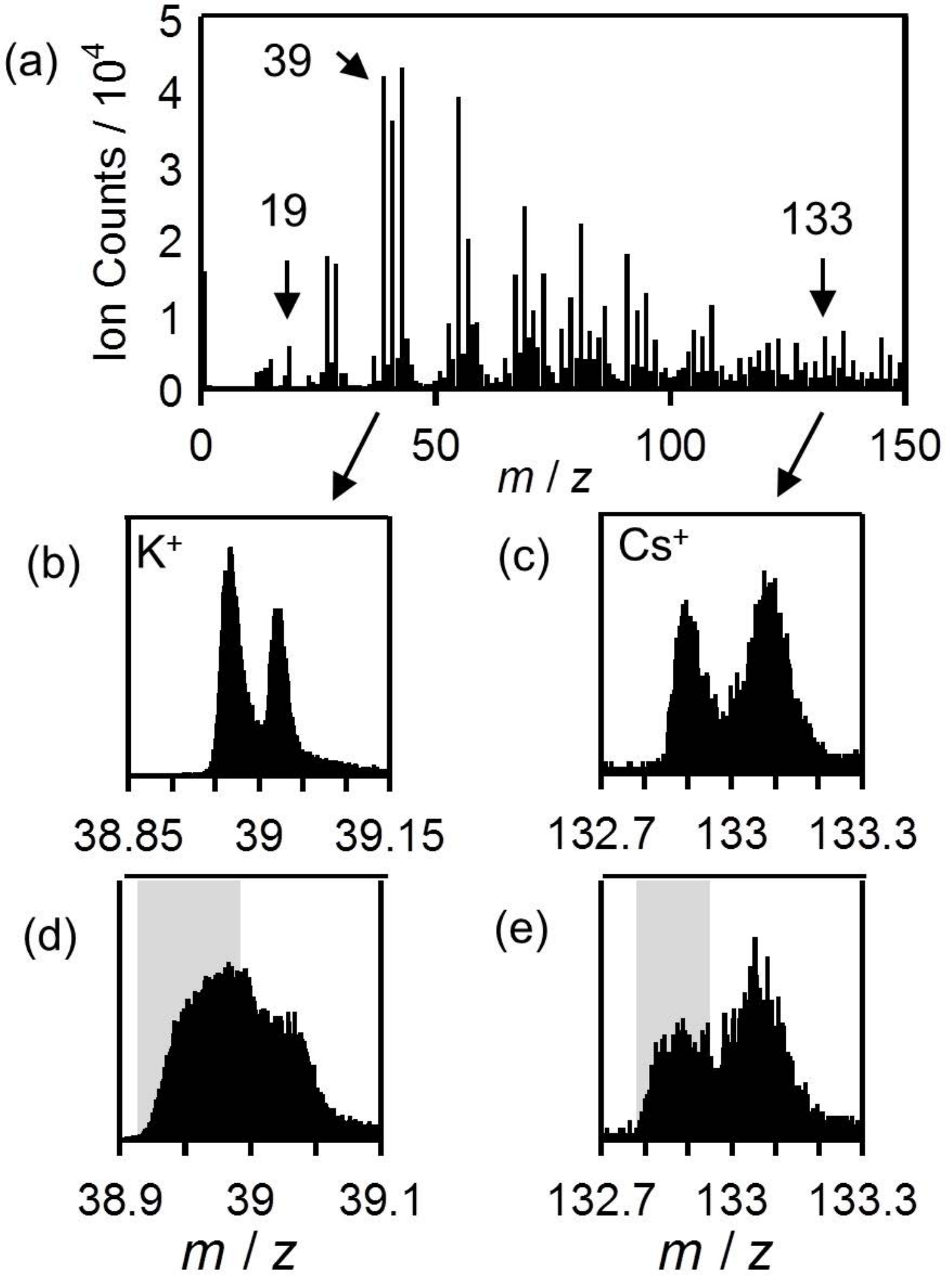
(a)
Ion Counts / 10^4
5
4
3
2
1
0
39
19
133
0
50
100
150
m / z
(b)
K+
38.85
39
39.15
(c)
Cs+
132.7
133
133.3
(d)
38.9
39
39.1
m / z
(e)
132.7
133
133.3
m / z

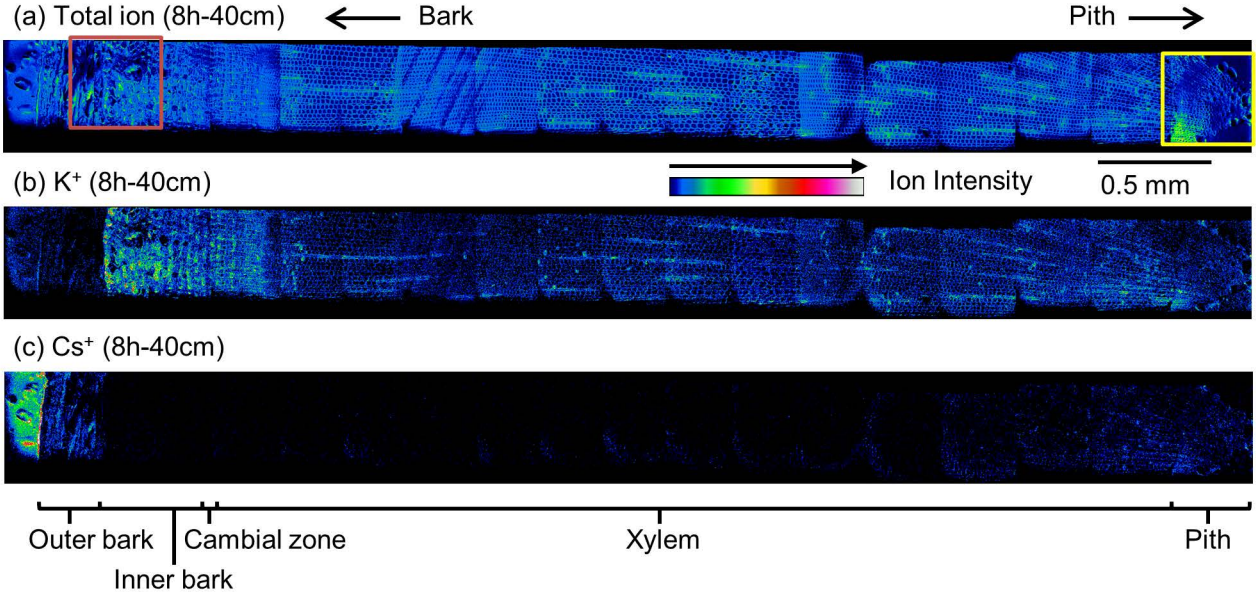

(d) Cryo-SEM image

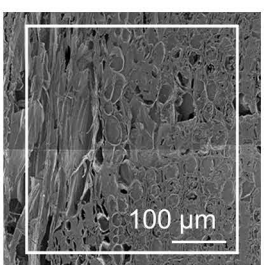

(e) Cs^+(blue) and K^+(red) overlay

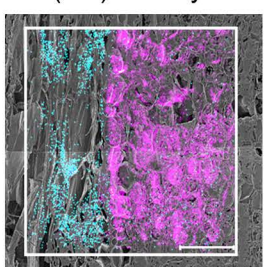

(f) Cryo-SEM image

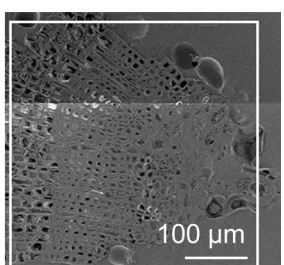

(g) Cs+(blue) overlay

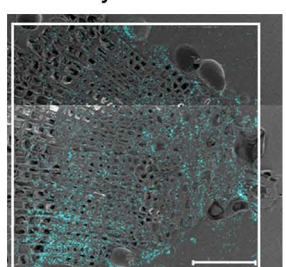

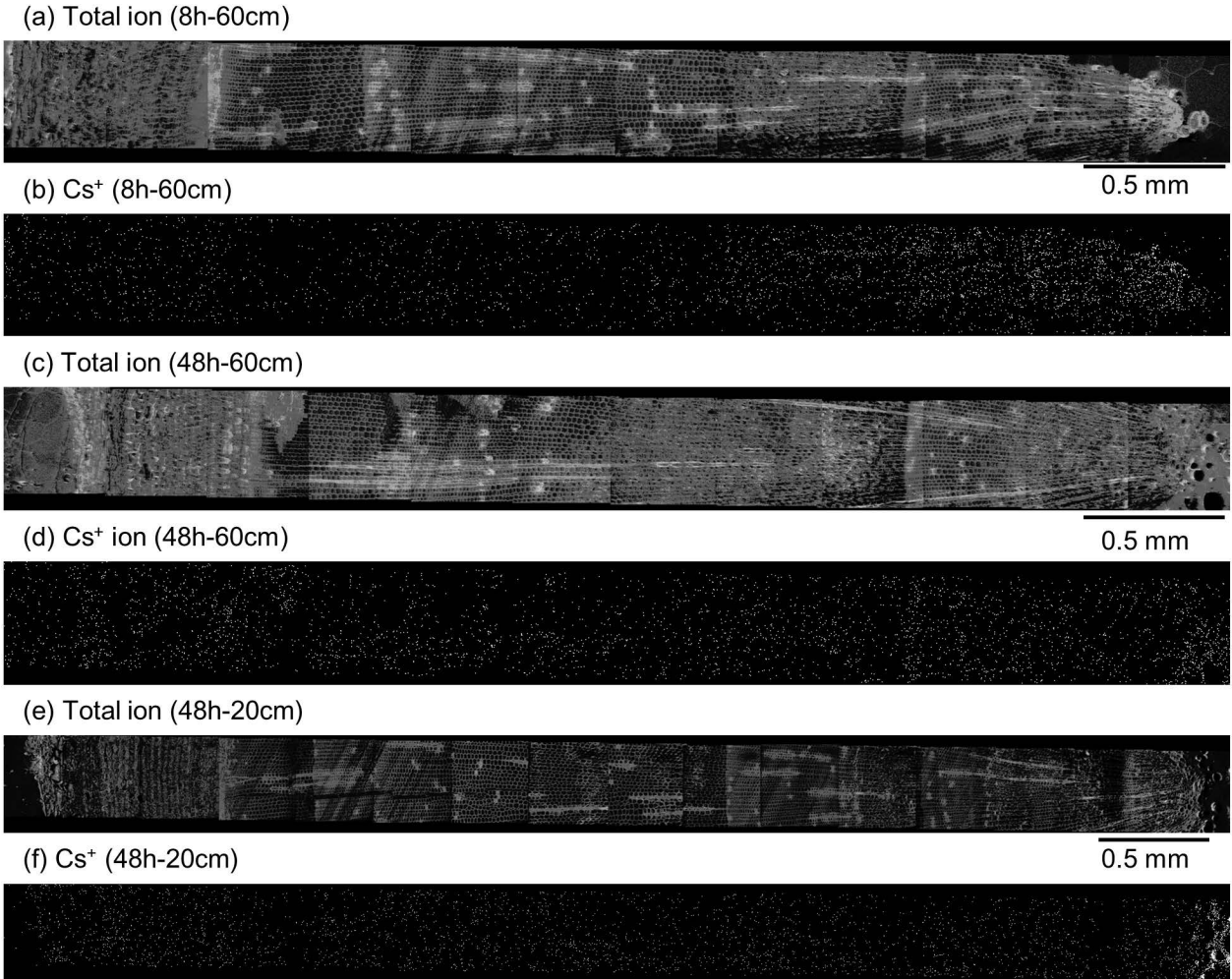
(a) Total ion (8h-60cm)
(b) Cs+ (8h-60cm)
0.5 mm
(c) Total ion (48h-60cm)
(d) Cs+ ion (48h-60cm)
0.5 mm
(e) Total ion (48h-20cm)
(f) Cs+ (48h-20cm)
0.5 mm

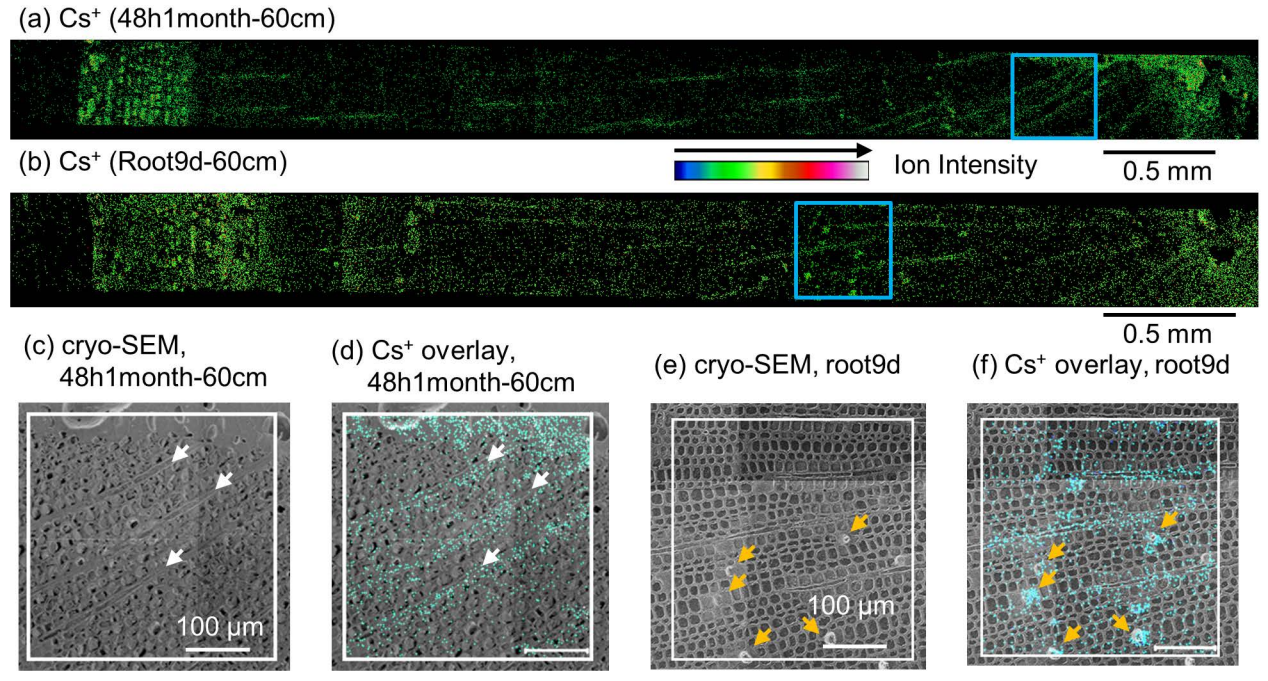
(a) Cs+ (48h1month-60cm)
(b) Cs+ (Root9d-60cm)
Ion Intensity
0.5 mm
0.5 mm
(c) cryo-SEM, 48h1month-60cm
(d) Cs+ overlay, 48h1month-60cm
(e) cryo-SEM, root9d
(f) Cs+ overlay, root9d
100 µm
100 µm

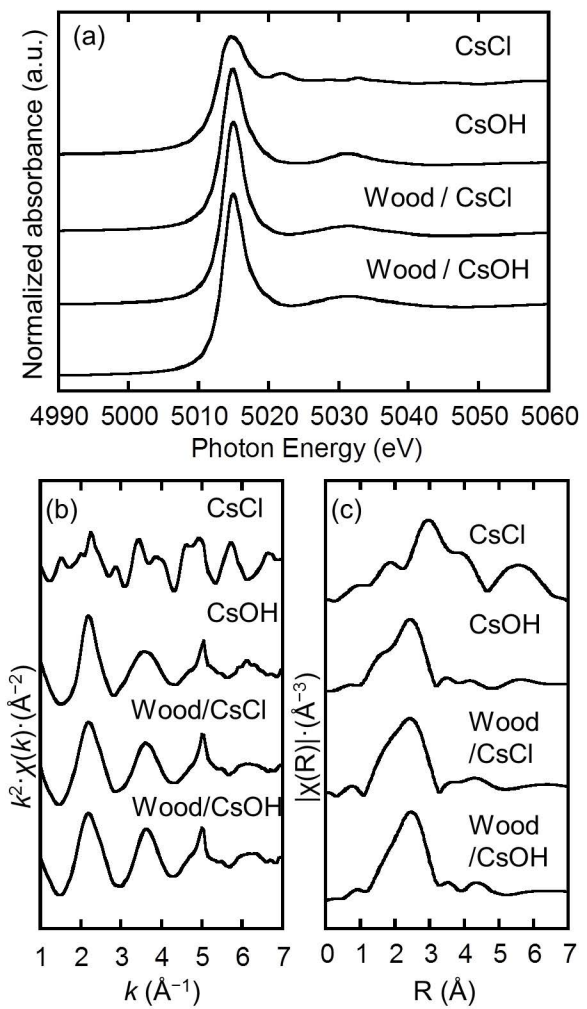
(a)
CsCl
CsOH
Wood / CsCl
Wood / CsOH
Normalized absorbance (a.u.)
4990 5000 5010 5020 5030 5040 5050 5060
Photon Energy (eV)
(b)
CsCl
CsOH
Wood/CsCl
Wood/CsOH
$k^2 \cdot \chi(k) \cdot (\text{Å}^{-2})$
1 2 3 4 5 6 7
k (Å^{-1})
(c)
CsCl
CsOH
Wood /CsCl
Wood /CsOH
$|\chi(R)| \cdot (\text{Å}^{-3})$
0 1 2 3 4 5 6 7
R (Å)